15TH IEA HEAT PUMP CONFERENCE
MAY 26–29, 2026 | HOFBURG
VIENNA 2026
DECARBONISATION THROUGH INNOVATION

Intermittent Refrigerant Mass Flow Rate Sensor for Enhanced Performance Monitoring of Heat Pumps

Michelle Makaroon[a], Cédric Teuillières[b], David Wiszniewski[b], Cong Toan Tran[a]*

[a] Center for Energy Environment and Processes (CEEP), Mines Paris, PSL Research University, 60 Boulevard Saint-Michel, 75006 Paris, FRANCE
[b] EDF R&D, Energy Efficiency Research & Technology Department (TREE), Avenue des Renardières, 77250 Ecuelles, FRANCE

Abstract

Heat pumps (HPs) are a key technology for the decarbonization of the building sector. To ensure their long-term contribution to climate goals, it is essential to evaluate their real-world performance - specifically their coefficient of performance (COP) and heating capacity - and enable robust diagnosis and control strategies. A critical parameter for this purpose is the refrigerant mass flow rate. While several non-intrusive on-field methods exist to estimate this quantity using limited measurements, their accuracy can degrade over time due to changes in performance of the HP components.

This study presents the development of a novel sensor system designed to intermittently measure the refrigerant mass flow rate in a HP circuit. Its objective is to provide a reliable reference measurement that can be used to verify and correct the output of available mass flow rate estimation methods. The device consists of an electrical heater applied to a refrigerant line, introducing a controlled thermal load into the HP circuit. By measuring the resulting temperature difference upstream and downstream of the device, the refrigerant flow rate can be calculated. As this process slightly disturbs normal operation of the HP, it is intended for periodic rather than continuous use.

The first part of this paper presents the thermal model of the sensor behind the mass flow rate measurement and the uncertainty calculation method. In the second part, the experimental set-up used for testing the sensor system is described. Finally, the results of the experimental validation are presented, highlighting the accuracy of this sensor system with a relative error ranging between 2.5 and 7 %, and an expanded uncertainty between 5 and 6 %.

This device enhances the robustness of online COP estimation methods and supports more accurate, real-time monitoring of heat pump performance under actual operating conditions.

©HPC2026.
Selection and/or peer-review under the responsibility of the organizers of the 15th IEA Heat Pump Conference 2026.

Keywords: flow rate; non-intrusive; on-field measurement; cost-effective; performance

1. Introduction

Fuel-fired heating accounts for approximately 75 % of total emissions arising from the building sector in France, or approximately 20 % of the country's greenhouse gas emissions [1]. Implementing solutions aimed for the enhancement of the heating equipments energy efficiencies is thus necessary. Heat pumps form good prospects for the energy transition in perspective. Among the various heat pump technologies, air-to-air heat pumps, used for heating and/or air conditioning, are the best-selling heat pumps with approximately 800,000 outdoor units sold per year in France [2]. Their use as primary heating is also expected to increase, forming an ideal solution for electric heaters substitution.

* Corresponding author. *E-mail address:* cong-toan.tran@minesparis.psl.eu

15th IEA Heat Pump Conference 2026 - ICO5.5 - https://doi.org/10.23697/4yt9-ng83

The actual COP of a heat pump can differ significantly from its nominal value, provided by the manufacturer, even for the same operating temperature conditions defined. During standardized tests, the compressor speed is set to achieve steady-state conditions, which differs from its actual operation in real conditions. Yang et al. [3] noted large differences between the on-field seasonal COP and that measured in the laboratory (ranging from 8 % to 32 %). In these dynamics of deployment of air-to-air heat pumps, and for the reasons previously mentioned, it is necessary to develop a reliable on-field method assessing the real performance of air-to-air heat pumps. The method can help verify the relevance of this HP technology as an essential tool for the energy transition. To develop such method, a major problem is linked to the complexity behind air vectors measurements, which makes most measurement methods unsuitable for long-term field implementation. Most methods often require bulky and intrusive devices which can be inconvenient for occupants and other equipments. Tran [4] developed an internal method based on the energy balance of the compressor. The mass flow rate of the refrigerant is computed through an assessment of the compressor heat losses, the measured electric compressor power and the enthalpy difference between the refrigerant suction and exhaust of the compressor. Most of the measurement sensors used are non-intrusive. This method has been tested in steady-state conditions within laboratory settings [5]. Noel [6] concludes that the compressor energy balance method measures the heat pump's performance with an accuracy of 5 % in steady-state conditions for conventional control heat pumps. Tran et al. [7] adapted this method for two-phase fluid at compressor suction (common condition in the case of the R32 refrigerant) in dynamic and stabilized conditions, with a relative uncertainty of 2 - 5 %. However, this method requires knowing the compressor's mapping, which can also degrade over time. Therefore, it is essential to develop a non-intrusive device used occasionally to make a correction if needed, through an on-field measurement of the refrigerant flow rate.

Among existing non-intrusive flow measurement technologies, ultrasonic flow meters constitute an interesting prospect. Sergey Mileiko et al. [8] proposed a delta time-of-flight based non-intrusive sensor system for ultrasonic flow rate metering. The system achieved a level of precision of ± 5.7 % and two different pipe diameters (15 mm and 22 mm) were used. Despite existing works in the literature for the development of non-intrusive ultrasonic sensors with good precision, this technology hasn't been proven for very small diameter applications. Also, most ultrasonic flow meters available in the market can't be used for very small pipe diameters, whereas in the residential heat pump sector, standard diameters for the highest power outputs are small (around 1.5 cm). Ultrasonic flow meters are also expensive, which defeats our initial purpose of having a simple way to measure the refrigerant flow rate.

Several studies addressed non-intrusive thermal flow meters, particularly for measuring low fluid flow rates. Cerimovic et al. [9] developed a non-invasive thermal flow sensor using a heater and two Pt100 temperature sensors on a 16 mm inner diameter pipe; the flow velocity is calculated from the heater's excess temperature empirically calibrated against a reference flow meter, with reported deviations of around 3 %. Despite this method being non-intrusive, and where only few watts in power are needed, it depends on careful calibration, and was only validated on water as an operating fluid.

Many machine learning enhanced flow meters have also emerged as a non-intrusive promising approach with very good precision. Amaral et al. [10] designed an intelligent non-intrusive thermal flow rate meter for small diameter applications, with 0.14 % full-scale error. The meter uses a copper duct and artificial intelligence is used to infer the flow rate from the thermal distribution on the duct surface. Vinicius David Fonseca et al. [11] developed an artificial neural network (ANN) model to deduct the mass flow rate of the refrigerant fluid in a refrigeration machine. The compressor speed, the refrigerant fluid specific mass, the evaporation and condensation temperatures of the refrigerant fluid were used as inputs for the ANN model. The average error was below 1 %. However, despite data being collected from seven different operation points in the latter, including transient response, this type of approach requires retraining or recalibration for every new setup, limiting generalizability in the case of deployment on various residential heat pump setups. Also, if the compressor mapping degrades with time, the heat pump's performance is affected, making this approach no longer reliable. Cong Li et al. [12] introduced an interesting study relying on the placement of fiber bragg grating (FBG) sensors on a pipe elbow to measure the strain difference caused by flow-induced pressure, which is quadratically related to flow velocity. The pipe diameter used for the validation of the apparatus is 8 mm, and shows interesting results with a maximum measurement error of 11.35 % in the five experiments conducted, however better precision is necessary if this method were to serve for verification purposes. Despite the existence of several methods for non-intrusive flow measurements, none are suitable in our case for the reasons mentioned above.

The objective of this paper is to present a simple, non-intrusive and cost-effective flow meter device. The design of this flow meter falls within the framework of providing a reference measurement to our on-field COP measurement method relying on the energy balance method, in heating, ventilation, and air conditioning (HVAC) applications. In our case, it is solely designed for verification processes, potentially allowing for correction of the compressor's volumetric efficiency when needed. The model is suitable and easily adaptable for various applications regarding flow rate measurements.

2. Method

2.1. Meter design and operating principle

The flow meter consists of an electrical resistor wrapped around a refrigerant tube, surrounded by an insulating layer. The device allows controlled thermal power to be injected into the refrigeration circuit. In the case of heat pump applications, the device requires to be located on the compressor's discharge line in order to develop a reliable thermal model; dealing with superheated vapor, eliminating constraints due to phase changes.

The flow meter relies on a thermal model where power input generates a temperature rise in the fluid. The refrigerant flow rate is then deducted by energy balance. In order to allow the refrigerant flow rate measurement by this method, the following information is needed: P_{elec} the electrical power, T_{in} and T_{out} the refrigerant temperatures at the upstream and downstream sides of the device, T_∞ the ambient temperature, p_{in} the refrigerant pressure, and also the geometrical and material properties parameters. Most of the latter are provided by the on-field method's apparatus, except for P_{elec} the electrical power and T_{out} the refrigerant outlet temperature downstream of the device. Also, the electrical power's measurement is not essential giving that we can calculate it using the values of the electrical resistance used and the sector voltage.

The thermal power of the heating film is partially lost in the atmosphere and the useful power transferred to the refrigerant can be expressed as:

$$P_{in} = \dot{m}_{ref} c_p \Delta T_{ref}, \tag{1}$$

where ΔT_{ref} is the difference between the refrigerant temperatures at the upstream and downstream sides of the device.

The thermal model behind the measurement of the flow rate by this method is described in the next subsection.

2.2. Thermal model

The 1D radial thermal model (Fig. 1) developed assumes steady state conditions. Dittus-Boelter's equation for heating is used for forced convection with the refrigerant flow [13]. The Churchill-Chu's correlation for a horizontal cylinder is used for natural convection with ambient air [14]. The correlations are given in Table 1.

Table 1. Correlations used for the convection coefficients

Dittus-Boelter [13]	Churchill-Chu [14]
$Re = 4\frac{\dot{m}}{\pi D \mu}$; $Pr = \frac{c_p \mu}{k}$	$Ra = \frac{g\beta \lvert T_s - T_\infty \rvert D_o^3}{\alpha \nu}$
$Nu = 0.023\, Re^{0.8} Pr^{0.4}$	$Nu = \left(0.6 + \frac{0.387\, Ra^{\frac{1}{6}}}{\left(1+\left(\frac{0.559}{Pr}\right)^{\frac{9}{16}}\right)^{\frac{8}{27}}}\right)^2$
$h = Nu\,\frac{k}{D}$	$h = Nu\,\frac{k}{D}$

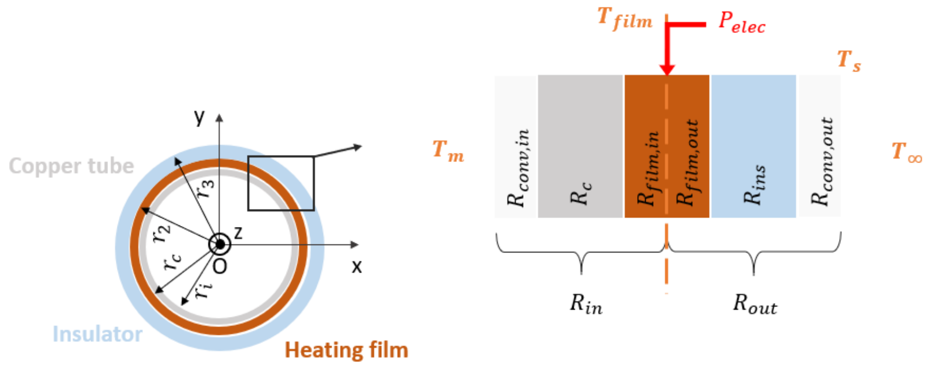

Figure 1. 1D radial thermal model and the equivalent thermal circuit

The refrigerant temperature in the heated zone is represented by its mean value $T_m = \frac{\Delta T_{ref}}{2} + T_{in}$, the axial heat flux being very small compared to the radial heat flux. The electrical power generated is applied at the film node, from which heat is distributed between the two branches, one leading to the refrigerant and the other to the atmosphere. The overall thermal circuit consists of a series of resistances corresponding to the successive conductive and convective layers. It is represented by two parallel branches, forming a thermal divider. The internal and external heat fluxes, with respectively R_{in} and R_{out} the equivalent inner and outer thermal resistances, are given by:

- The internal heat flux:

$$P_{in} = \frac{T_{film} - T_m}{R_{in}} \tag{2}$$

- The external heat flux:

$$P_{out} = \frac{T_{film} - T_\infty}{R_{out}} \tag{3}$$

The electrical power being equal to the sum of the internal and external fluxes (Eq. (2) and Eq. (3)), the internal flux can also be expressed as:

$$P_{in} = \frac{R_{out} P_{elec} + (T_\infty - T_m)}{R_{in} + R_{out}} \tag{4}$$

Radial heat conduction follows a logarithmic variation with radius, the heating film is partitioned into two symmetrical half-sections, defined by the geometric mean radius $r_m = \sqrt{r_c r_2}$. This configuration yields two identical half-resistances, reflecting the logarithmic symmetry inherent to cylindrical heat conduction. Note that $r_2 = r_c + t_{film}$, $r_3 = r_2 + t_{ins}$ and $D_o = 2r_3$ (t_{film} and t_{ins} being the film thickness and that of the insulator respectively). The individual thermal resistances are expressed in Table 2.

Table 2. Thermal resistances

Thermal resistance	Equation	Heat transfer
$\boldsymbol{R_{conv,in}}$	$\frac{1}{h_i 2\pi r_i L}$	Inner convection (fluid)
$\boldsymbol{R_c}$	$\frac{\ln\left(\frac{r_c}{r_i}\right)}{2\pi k_c L}$	Copper conduction
$\boldsymbol{R_{film,in}}$	$\frac{\ln\left(\frac{r_m}{r_c}\right)}{2\pi k_{film} L}$	Inner half of the film conduction
$\boldsymbol{R_{film,out}}$	$\frac{\ln\left(\frac{r_2}{r_m}\right)}{2\pi k_{film} L}$	Outer half of the film conduction
$\boldsymbol{R_{ins}}$	$\frac{\ln\left(\frac{r_3}{r_2}\right)}{2\pi k_{ins} L}$	Insulation conduction
$\boldsymbol{R_{conv,out}}$	$\frac{1}{h_o 2\pi r_3 L}$	Outer convection (air)

The equivalent thermal resistances R_{in} and R_{out} are expressed as:

$$R_{in} = R_{conv,in} + R_c + R_{film,in} \tag{5}$$

$$R_{out} = R_{film,out} + R_{ins} + R_{conv,out} \tag{6}$$

The thermal model developed relies on the numerical solution of a system of 3 equations, with the following variables as unknowns: $\dot{m}_{\mathrm{ref}}$ the refrigerant mass flow rate, h_o the convective heat transfer coefficient (convection with ambient air), and T_s the outer surface temperature of the device.

The system is ruled by the following equations:

$$\begin{cases} \dot{m}_{ref} c_p \Delta T_{ref} - \dfrac{R_{out} P_{elec} + (T_\infty - T_m)}{R_{in} + R_{out}} = 0 & (7) \\ h_o - Nu \dfrac{k_{air}}{D_o} = 0 & (8) \\ T_s - \left(T_\infty + P_{out} R_{conv,out}\right) = 0 & (9) \end{cases}$$

The solution of the system of equations allows the determination of the refrigerant mass flow rate.

2.3. Outlet temperature adjustment

In our study, while the inlet temperature sensor is placed exactly at the inlet of the heating film, the outlet temperature sensor is at the condenser inlet, which is quite far from the heating film. In this case, heat losses across the refrigerant pipe can distort the outlet temperature measurement. For instance, we can see in Fig. 2 the inlet temperature being greater than at the outlet before the heating phase starts.

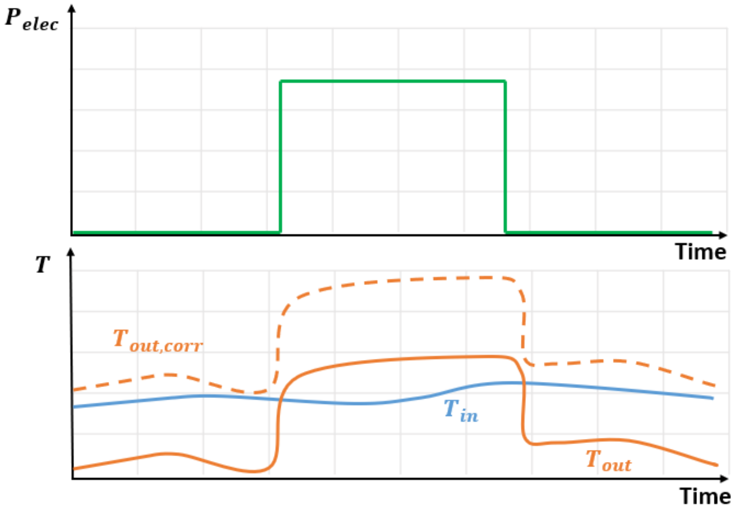

Figure 2. Electrical power, sensor inlet and outlet temperatures evolutions

The heat losses being proportional to the temperature difference between the fluid and the ambient temperature, we choose to correct the output temperature by applying the following linear scaling with respect to the ambient temperature, where the 0 index corresponds to the temperature prior to the heating phase:

$$T_{out,corr} = T_{out} + \frac{(T_{in,0} - T_{out,0})(T_{out} - T_{\infty})}{T_{out,0} - T_{\infty,0}} \tag{10}$$

2.4. Uncertainty calculation

In the experimental setup of this study, the refrigerant temperatures upstream and downstream of the measurement device are not obtained from direct measurements in the fluid. Instead, contact sensors are attached to the external wall of the refrigerant tube. This measurement configuration inherently introduces a systematic bias, as the wall temperature is generally lower than the true fluid temperature due to thermal resistances and imperfect thermal coupling between the sensor and the tube. As a result, the measured temperature consistently underestimates the true refrigerant temperature. This systematic deviation must therefore be explicitly modelled and clearly separated from random sensor noise to obtain a reliable uncertainty estimate on the mass flow rate.

The method developed here aims to quantify the uncertainty of the mass flow rate computed by the method, by accounting for both classical measurement uncertainties and the specific biases associated with wall-mounted temperature sensors. For each measurement point, the true temperatures are modelled as:

$$T_{true} = T_{meas} + b + \varepsilon \tag{11}$$

where ε is the intrinsic Gaussian sensor noise, and b the systematic bias associated with the wall–refrigerant temperature difference. To represent correlations between the inlet and outlet sensors, the bias is decomposed into a common component b_c affecting both sensors identically, and a differential component b_d capturing asymmetries between the two mounting conditions. Both components are assumed Gaussian and independent. An important consequence is that only the differential bias affects the temperature difference ΔT_{ref}, while the common bias shifts only the absolute temperature levels.

All input quantities of the measurement method (X_j) are gathered into a covariance matrix M. Classical measurement variables (electrical power, inlet pressure, geometry parameters, etc.) are treated as independent Gaussian variables. For the inlet and outlet temperatures, a transformation to ΔT_{ref} and T_m (mean temperature) is used. The expectations and variances of these variables follow directly from the bias model (μ_c, μ_d, σ_c, σ_d) and from the sensor noise.

The sensitivities $\left(\frac{\partial \dot{m}_{ref}}{\partial x_j}\right)$ are computed numerically through finite differences around an operating point by perturbing each input by a representative amount equal to its standard deviation. The resulting gradient vector J is then used to propagate uncertainties:

$$u^2(\dot{m}_{ref}) \approx J\, M\, J^T \tag{12}$$

This propagation allows a clear separation between systematic correction (handled explicitly) and random uncertainty (handled statistically).

3. Experimental Validation

3.1. Experimental setup

The measurements serving for the validation of this device were carried on a mono-split air-to-air heat pump with a rotary compressor. It works on R32 and has a heating capacity of 3.6 kW.

The heat pump is operating in laboratory conditions. It is placed in two climatic cells, allowing the simulation of the desired operating conditions. It is only working in full load mode even though a variable speed compressor is used, due to experimental constraints. The exterior temperature T_{ext} is relatively constant, and T_∞ the ambient temperature is varied in order to test the apparatus in different operating points. However, the heat pump being in full load operation all the time, the refrigerant mass flow rate doesn't vary significantly.

The developed device is positioned between the Coriolis mass flow rate meter, used for reference measurements, and the interior unit, on the gas line at the condenser inlet. All the elements used for the on-field measurement method of the heat pump performance are deployed. In particular, the refrigerant pressure is already measured. The outlet refrigerant temperature downstream of the device is provided through the Pt100 probe positioned at the condenser inlet. For the purpose of flow rate measurement, an additional Pt100 probe was used to measure the temperature upstream of the device. Note that, the temperature measurements of the refrigerant, upstream and downstream of the device, do not correspond exactly to the inlet and outlet of the device and there may be significant heat losses between these two measurement points. Also, an additional wattmeter is needed for the electric power measurement of the heating film.

The estimated uncertainties of the different sensors/measurements are provided in Table 3. The surface-mounted PT100 sensors have a nominal uncertainty of about 0.1 K, but the indirect measurement on the tube wall leads to a larger effective uncertainty on the true fluid temperature. This uncertainty is estimated at 0.8 K [15]. We suppose a common bias of 0.6 K and a differential component of 0.2 K. Uncertainties associated with the heat-transfer correlations and the computation of refrigerant properties are not included in this study. The measurement recording step is of 10 s.

Table 3. Input quantities and associated standard uncertainties (1σ)

Quantity	Unit	Uncertainty
Refrigerant temperature:	K	
• Sensor uncertainty		• 0.1
• Common bias		• $\mu_c = 0.6, \sigma_c = 0.2$
• Differential bias		• $\mu_d = 0.0, \sigma_d = 0.2$
Electrical power	W	1 %
Pressure	bar	0.2
Thermal conductivity	W/(m.K)	
• Copper		• 5
• Film		• 0.05
• Insulation		• 0.005
Geometrical parameters (L, D, etc.)	mm	0.5

3.2. Results

3.2.1. Temperature response

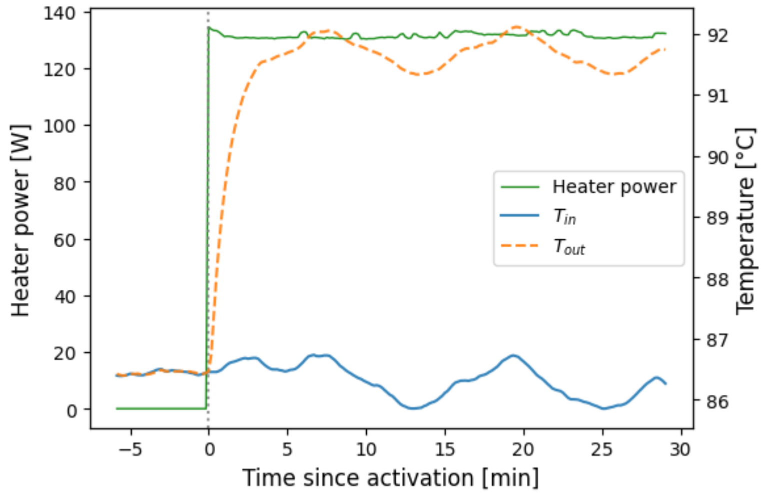

Figure 3. Heater power, inlet and outlet temperatures evolutions during heating phase

Fig. 3 shows the time evolution of the heater electrical power (P_{elec}) together with the measured inlet and outlet temperatures during a representative heating sequence. At the beginning of the test, the heater is inactive (P_{elec} close to zero), and the inlet and outlet temperatures are identical.

When the heater is switched on, its electrical power quickly reaches a nearly constant value. In response to the applied thermal load, the outlet temperature (T_{out}) begins to rise while the inlet temperature (T_{in}) remains mostly unchanged. The temperature difference between the two sensors increases progressively during this transient phase.

After approximately 5 to 10 minutes, T_{out} tends toward a quasi-steady value. However, instead of forming a perfectly stable plateau, T_{out} shows small fluctuations. These oscillations closely follow those observed on T_{in}, indicating that both temperatures are affected by slow variations in the operating conditions of the heat pump. As a consequence, the temperature difference stabilizes around a mean value but remains subject to the same underlying fluctuations.

This behavior confirms that the thermal excitation produced by the heater generates a clear increase in outlet temperature, while also showing that the sensor reacts to the natural variability of the refrigerant temperature.

It should be noted that the measured outlet temperature (T_{out}) is initially about 2 °C lower than the inlet temperature (T_{in}). This offset is caused by thermal losses along the refrigerant pipe and highlights the need for the specific temperature adjustment described in Section 2.3. Without this correction, the performance of the device would be significantly degraded, especially considering that the temperature rise induced by the heater is only on the order of 6 °C.

3.2.2. Identification of a stable measurement period

After heater activation, the heat pump exhibits internal and external fluctuations that affect the measured temperatures and the calculated mass flow rate. Since the flow calculation requires a quasi-steady regime, an automatic method is used to select a stable period.

The procedure is based on a number of chosen measurable variables, such as the outlet temperature. A sliding window of fixed duration (5 minutes) is moved through the data, and a stability metric (standard deviation) is computed for each window. The first window whose metric is below a predefined threshold is selected.

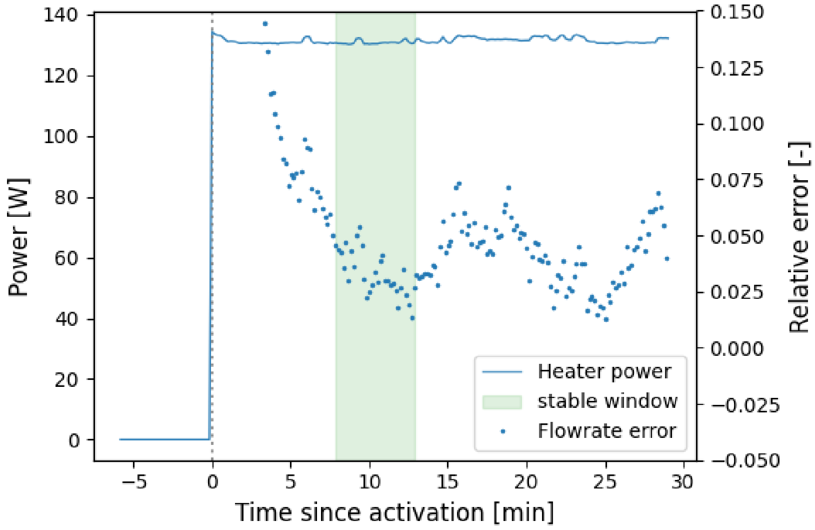

Figure 4. Relative error of the mass flow rate during heating phase

Fig. 4 shows the relative error between the calculated mass flow rate and the Coriolis reference. Immediately after activation, the error is large due to transient thermal conditions. Once a stable regime is reached, the error fluctuates between approximately 2.5 and 5 %. The identified stable period, highlighted in the figure, is then used for the final flow rate evaluation.

3.2.3. Relative error

To assess the robustness of the method, several tests were conducted under different operating conditions. As the heat pump operated at full capacity in all cases, the thermal power remained close to its maximum value and the refrigerant mass flow rate stayed within a relatively narrow range.

Fig. 5 shows the relative error between the calculated mass flow rate and the Coriolis reference as a function of the inlet temperature (T_{in}) for five distinct operating points. For each test, the error bar represents the standard deviation of the error calculated over the automatically selected stable period.

The standard deviation is very small for all tests, confirming both the repeatability of the measurement and the effectiveness of the stability-selection method. Depending on the operating point, the mean relative error ranges from 2.5 to 7 %, which is fully acceptable for the intended application and demonstrates that the device provides reliable reference measurements across the tested conditions.

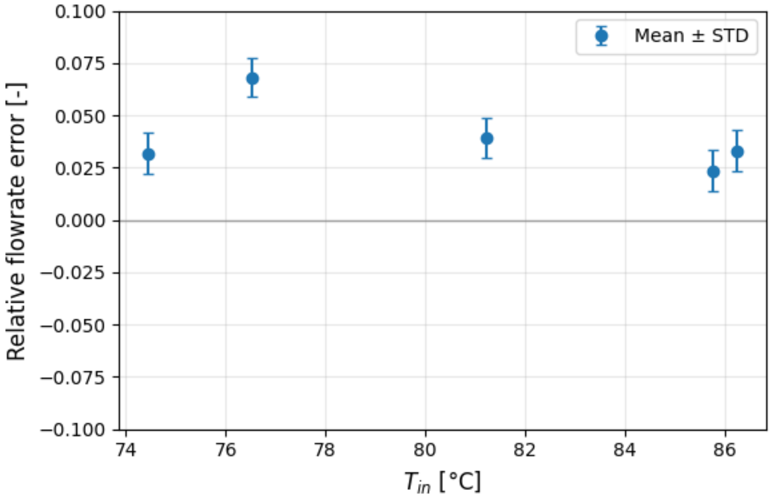

Figure 5. Relative error of the mass flow rate with respect to the inlet temperature

3.2.4. Uncertainty

The uncertainty on the calculated mass flow rate was evaluated using the propagation method described earlier. Since the uncertainty structure is very similar across all operating conditions, the results are presented for a representative test point. For this point, the expanded uncertainty (k = 2) on the mass flow rate lies between 5 and 6 %.

The uncertainty is strongly dominated by the temperature measurements. The inlet and outlet temperature channels each account for approximately 46 % of the total uncertainty. The contribution of the electrical power measurement is much smaller, around 4 %. All remaining input quantities, including fluid properties and geometric parameters, jointly contribute to the remaining 4 %. This confirms that the accuracy of the temperature difference is the key factor limiting the performance of the method.

This estimate is slightly optimistic, as it does not include the uncertainty associated with convection-based thermal corrections, whose coefficients are derived from empirical correlations that carry their own uncertainty. On the other hand, the uncertainty is expected to decrease under part-load operation, where the refrigerant mass flow rate is lower and the temperature rise across the heater is larger, improving the sensitivity of the method. This trend is particularly relevant for real-world applications, where part-load operation is predominant.

Importantly, the calculated uncertainty is fully consistent with the experimental relative errors observed in the previous sections, which ranges from 2.5 to 7 %. This agreement provides strong support for the validity of the uncertainty model and for the reliability of the measurement device.

3.2.5. Discussion

The total duration required to obtain a valid measurement with the proposed device is approximately 10 minutes: about five minutes for the temperature response to reach a quasi-steady regime, followed by a five-minute stable period identified by the selection algorithm. Such a duration is fully acceptable for the intended use of the device, which is designed to operate intermittently.

The influence of the device on the heat pump operation appears to be very limited. As shown previously, the inlet temperature exhibits small fluctuations after heater activation. It is not possible to determine unequivocally whether this behavior originates from intrinsic dynamics of the heat pump or from the thermal excitation introduced by the device. In any case, the magnitude of the fluctuation remains very small, typically within ± 0.5 K. This is consistent with the fact that the electrical heating power is negligible compared with the thermal capacity of the heat pump. Overall, the device perturbs the system only minimally while still generating a clear and exploitable temperature response for mass flow rate estimation.

In this study, the thermal model was presented in a detailed form to ensure that the method remains applicable to a wide range of systems and operating conditions. However, for a given system in which the expected ranges of mass flow rate, pressure, and temperature are known in advance, the model can be significantly simplified. In such cases, the mass flow rate could be computed directly from pre-identified relationships without solving a full set of coupled equations, reducing computational effort and enabling faster implementation.

4. Conclusion

This work presented the development and experimental validation of an intermittent device for measuring the refrigerant mass flow rate in a heat pump circuit. The method relies on applying a small and controlled thermal excitation to the refrigerant line and estimating the mass flow rate from the resulting temperature rise. The device was shown to produce a clear and repeatable thermal response. Across several operating conditions, the relative error remained between 2.5 and 7 %, while the expanded uncertainty of the method was estimated between 5 and 6 %, in good agreement with the experimental observations. The device perturbs the heat pump only minimally and requires about ten minutes to obtain a valid measurement, which is adequate for intermittent use.

A key advantage of the proposed approach is that it is entirely non-intrusive: it requires no modification of the refrigerant loop and relies only on low-cost surface-mounted temperature sensors (PT100). This makes the device easy to install, inexpensive, and suitable for integration in both laboratory and real-world systems.

Future work will investigate the performance of the device under part-load operation, where lower mass flow rates are expected to increase the temperature rise and improve the measurement accuracy. Additional efforts will also focus on refining the thermal model, especially the treatment of convection-related uncertainties, and on integrating the device into real-time frameworks for periodic calibration of non-intrusive mass flow estimators.

Acknowledgments

This work falls within the framework of a wider project for the development of an on-field measurement method of the performance of heat pumps, funded by ADEME (Agence de la transition écologique).

Nomenclature

Latin symbols

L	Flow meter length	(m)
r_i	Internal radius of the tube	(m)
r_c	External radius of the tube	(m)
t	Thickness	(m)
k	Thermal conductivity	(W/m.K)
p	Pressure	(Pa)
c_p	Specific heat capacity at constant pressure	(J/kg.K)
T	Temperature	(K)
P	Power	(W)
$\dot{m}$	Mass flow rate	(kg/s)
g	Gravity acceleration	(m/s^2)
h	Convection coefficient	(W/m^2.K)
R	Thermal resistance	(K/W)
Re	Reynolds number	
Pr	Prandtl number	

Ra	Rayleigh number	
Nu	Nusselt number	

Greek symbols

μ	Dynamic viscosity	(kg/m.s)
β	Thermal expansion coefficient	(K^{-1})
ν	Kinematic viscosity	(m^2/s)
α	Thermal diffusivity	(m^2/s)

Superscripts and subscripts

ref	refrigerant
m	mean
meas	measured
∞	ambient
elec	electrical
s	surface
i	inner
o	outer
c	copper
ins	insulator
conv	convection

References

[1] RTE, 2020. “Réduction des émissions de CO_2, impact sur le système électrique : Quelle contribution du chauffage dans les batiments à l’horizon 2035 ?”.

[2] Ministère de la transition énergétique, 2022. “Ventes annuelles de pompes à chaleur (pac) individuelle”.

[3] Yang, Z., Ding, L., Xiao, H., Wang, B., & Shi, W, 2021. “Field performance of household room air conditioners in yangtze river region in china: Case studies,” *Journal of Building Engineering*, 34. https://doi.org/10.1016/j.jobe.2020.101952.

[4] Tran, C., 2012. “Méthodes de mesure in situ des performances annuelles des pompes à chaleur air/air résidentielles,” Doctoral Dissertation, Mines Paristech, PSL Research University.

[5] Tran, C., Riviere, P., Marchio, D., & Arzano-Daurelle, C., 2013. “In situ measurement methods of air-to-air heat pump performance,” *IJF*, 36(5), 1442–1455. http://dx.doi.org/10.1016/j.ijrefrig.2013.03.021.

[6] Noël, D., 2020. “Validation et extension d’une méthode de mesure embarquée des performances des pompes à chaleur,” Doctoral Dissertation, Mines ParisTech, PSL Research University.

[7] Makaroon, M. , Noël, D., Cauret, O., Tran, C.T., 2025. “On-field measurement method for the coefficient of performance of air-to-air heat pumps considering wet compression and dynamic operating conditions,” ECOS 2025.

[8] Mileiko, S., Cetinkaya, O., Yakovlev, A., Balsamo, D., 2021. “A Non-intrusive Ultrasonic Sensor System for Water Flow Rate Measurement,” 2021 IEEE Sensors Applications Symposium (SAS). https://doi.org/10.1109/SAS51076.2021.9530165.

[9] Cerimovic, S., Treytl, A., Glatzl, T., Beigelbeck, R., Keplinger, F., Sauter, T., 2019. “Development and Characterization of Thermal Flow Sensors for Non-Invasive Measurements in HVAC Systems,” *Sensors*, 19(6), 1397. https://doi.org/10.3390/s19061397.

[10] Amaral, J.L.M., Quirino, T.M., Quirino, J.M., Silva, J.R.C., 2025. “Intelligent non-intrusive thermal flow rate meter designed for small diameter applications,” *Flow measurement and Instrumentation*, 104, 102902. https://doi.org/10.1016/j.flowmeasinst.2025.102902.

[11] Fonseca, V.D., et al., 2022. “Mass flow prediction in a refrigeration machine using artificial neural networks,” *Applied Thermal Engineering*, 214, 118893. https://doi.org/10.1016/j.applthermaleng.2022.118893.

[12] Li, C., Liu, M-Y., Song, H., Yang, X-L., Wu, Y-H. “A Non-Invasive Measurement Method of Pipeline Flow Rate Based on Dual FBG Sensors,” *IEEE Sensors Journal*, 22 (6), 5669-5677. https://doi.org/10.1109/JSEN.2022.3141733.

[13] Dittus, F.W., Boelter, L.M.K., 1930. “Heat transfer in automobile radiator of the tubular type,” *University of California at Berkley Publ. Eng.2,* 443-461.

[14] Churchill, S., Chu, H., 1975. “Correlating equations for laminar and turbulent free convection from a horizontal cylinder,” *International Journal of Heat and Mass Transfer,* 18 (9), 1049-1053. http://dx.doi.org/10.1016/0017-9310(75)90222-7.

[15] LNE, 2004. “Guide d'utilisation des capteurs de température de surface,” Projet AQCEN, Ministère de l'Economie des Finances et de l'Industrie, Laboratoire national de métrologie et d'essais.